# Macrophage-fibroblast crosstalk drives Arg1-dependent lung fibrosis via ornithine loading


**Authors**

Preeti Yadav[1,2], Javier Gómez Ortega[1,2], Whitney Tamaki[3,4], Charles Chien[5,6], Kai-chun Chang[7], Nivedita Biswas[1,2], Sixuan Pan[8], Julia Nilsson[9], Xiaoyang Yin[1,2,10], Aritra Bhattacharyya[1,2], Kaveh Boostanpour[1,2], Tanay Jujaray[1,2], Jasper Wang[1,2], Tatsuya Tsukui[1,11], Dean Sheppard[1,11], Baosheng Li[10], Mazharul Maishan[1], Hiroki Taenaka[1], Michael A. Matthay[1], Rieko Muramatsu[12], Lenka Maliskova[13], Arnab Ghosh[13], Walter L. Eckalbar[13], Ari B. Molofsky[9], Paul J. Wolters[1], Stanley J. Tamaki[13], Trever Bivona[3,4,14], Adam R. Abate[8], Allon Wagner[5,6,15], Kevin M. Tharp[16], Mallar Bhattacharya[1,2§]

**Affiliations**

[1]Division of Pulmonary, Critical Care, Allergy, and Sleep, Department of Medicine, University of California, San Francisco, San Francisco, CA, USA

[2]Sandler Asthma Basic Research Center, University of California, San Francisco, San Francisco, CA, USA

[3]Department of Medicine, University of California, San Francisco, San Francisco, CA 94158, USA.

[4]Helen Diller Family Comprehensive Cancer Center, University of California, San Francisco, San Francisco, CA 94158, USA.

[5]Department of Electrical Engineering and Computer Sciences, University of California, Berkeley, CA 94720, USA

[6]Center for Computational Biology, University of California, Berkeley, CA 94720, USA

[7]Twist Bioscience, 681 Gateway Blvd, South San Francisco, CA, USA

[8]Department of Bioengineering and Therapeutic Sciences, University of California, San Francisco, San Francisco, CA, USA

[9]Department of Laboratory Medicine, University of California, San Francisco, San Francisco, CA, USA

[10]Department of Radiation Oncology, Shandong Cancer Hospital and Institute, Shandong First Medical University and Shandong Academy of Medical Sciences, Jinan, China

[11]Cardiovascular Research Institute; University of California, San Francisco, San Francisco, CA, USA

[12]Department of Molecular Pharmacology, National Institute of Neuroscience, National Center of Neurology and Psychiatry, Kodaira, Japan

[13]UCSF CoLabs, University of California, San Francisco, San Francisco, CA 94143, USA

[14]Chan-Zuckerberg Biohub, San Francisco, CA 94158, USA.

[15]Department of Molecular and Cell Biology, University of California, Berkeley, CA 94720, USA

[16]Cancer Metabolism and Microenvironment Program, NCI-Designated Cancer Center, Sanford Burnham Prebys Medical Discovery Institute, La Jolla, CA, USA

**Declaration of Interests**

The authors have no conflicting financial interests.

**Contact Info**

§ Correspondence: mallar.bhattacharya@ucsf.edu

**Abstract**

Monocyte-derived macrophages recruited to injured tissues induce a maladaptive fibrotic response characterized by excessive production of collagen by local fibroblasts. Macrophages initiate this programming via paracrine factors, but it is unknown whether reciprocal responses from fibroblasts enhance profibrotic polarization of macrophages. We identify macrophage-fibroblast crosstalk necessary for injury-associated fibrosis, in which macrophages induced interleukin 6 (*IL-6*) expression in fibroblasts via purinergic receptor P2rx4 signaling, and IL-6, in turn, induced arginase 1 (*Arg1*) expression in

macrophages. Arg1 contributed to fibrotic responses by metabolizing arginine to ornithine, which fibroblasts used as a substrate to synthesize proline, a uniquely abundant constituent of collagen. Imaging of idiopathic pulmonary fibrosis (IPF) lung samples confirmed expression of *ARG1* in myeloid cells, and arginase inhibition suppressed collagen expression in cultured precision-cut IPF lung slices. Taken together, we define a circuit between macrophages and fibroblasts that facilitates cross-feeding metabolism necessary for injury-associated fibrosis.

**Keywords**

Macrophages; Fibroblasts; Fibrosis; IPF; Arginase 1; Ornithine

## Introduction

Pathologic fibrosis is a destructive response to tissue injury that results from the deposition of excess fibrillar collagen by activated fibroblasts. Recent studies have revealed a heterogeneity of fibroblast states following injury, and inflammatory fibroblasts have been detected as a distinct subset of mesenchymal cells present in the early period after injury prior to the onset of full-blown fibrosis[1, 2, 3]. However, how cytokine expression by inflammatory fibroblasts regulates fibrosis is not well understood.

The early phase of injury is also marked by an influx of monocyte-derived macrophages, which localize to fibroblasts at sites of injury[4]. Several studies have shown that these monocyte-derived macrophages signal to fibroblasts via paracrine mediators[4, 5, 6], but the resulting crosstalk between the two cell types that may orchestrate the fibrotic progression is not well characterized. Here, we identify a paracrine circuit between macrophages and fibroblasts that is established in the late inflammatory phase following tissue injury. In a tissue injury model, macrophage-derived extracellular ATP drove fibroblast IL-6 expression. IL-6, in turn, induced macrophage expression of Arg1, which was necessary for lung collagen production via ornithine metabolism by activated fibroblasts.

## Results

77 ***Extracellular ATP signaling via P2rx4 regulates fibroblast IL-6 expression.***

78 To screen for macrophage-dependent secreted factors expressed by fibroblasts, we analyzed scRNAseq
79 data from cocultures of primary lung macrophages and fibroblasts, or fibroblasts cultured alone (**Figure**
80 **1a-b, Figure S1a-b**). This analysis revealed the induction of multiple clusters unique to fibroblasts
81 cocultured with macrophages (**Figure 1c**). Notably, these clusters had higher levels of a gene signature
82 for collagen genes (**Figure S1c, Table S1**), consistent with the pro-fibrotic effects of macrophage
83 coculture. Focusing analysis on secreted factors[7], we also noted high expression of the cytokine IL-6 in
84 macrophage coculture-specific fibroblast clusters (**Figure 1d**; **Figure S1d**). IL-6 has emerged as a target
85 for the treatment of lung fibrosis[8, 9, 10, 11]. Analysis of scRNAseq time course data for multiple lung cell
86 types in the bleomycin model confirmed that IL-6 was most highly expressed in fibroblasts *in vivo* (**Figure**
87 **1e**), with some expression also noted in other mesenchymal cells such as smooth muscle cells and
88 pericytes (**Figure S1e**). We then confirmed macrophage-dependent fibroblast IL-6 induction in cocultures
89 derived from deceased donor human lungs (**Figure S1f**).

90 To determine the mechanism of IL-6 induction in fibroblasts, we interrogated GO datasets under
91 the category of "Cellular Response to Stimulus" to detect dominant stimulus-based pathways that could
92 be attributable to the presence of macrophages. This analysis revealed that the GO pathway "Cellular
93 Response to ATP" was enriched in fibroblasts when they were cocultured with macrophages (**Figure 1f**).
94 This GO pathway is relevant because extracellular ATP (eATP) levels are elevated in the bronchoalveolar
95 lavage fluid of patients with idiopathic pulmonary fibrosis (IPF)[12]. Furthermore, we had previously
96 reported that fibroblast-specific deletion of the eATP receptor P2rx4 in mice suppresses injury-induced
97 fibrosis[13]. In that work, we also found that P2rx4 was the most highly expressed receptor for ATP among
98 the 7-member P2rx family in lung fibroblasts.

99 To test if eATP signaling via P2rx4 regulates IL-6 expression, we assayed IL-6 levels by ELISA
100 of conditioned media from cocultures of WT macrophages with either WT or P2rx4 knockout (KO)
101 fibroblasts, finding that IL-6 was decreased in the case of P2rx4 KO fibroblasts (**Figure 1g**). Direct
102 treatment of cultured murine lung fibroblasts with ATPγS, a nonhydrolyzable form of ATP, increased IL-

103 6 in the conditioned media of WT but not P2rx4 KO lung fibroblasts (**Figure S2a**). This effect was blocked
104 by inhibition of p38 Map Kinase, which has been shown to mediate P2rx4 signaling[14, 15] (**Figure S2b**).
105 Importantly, mice with fibroblast-specific P2rx4 KO had decreased bronchoalveolar lavage IL-6 compared
106 to wild type following bleomycin injury (**Figure 1h**), and siRNA KD of P2RX4 in human lung fibroblasts
107 decreased IL-6 expression (**Figure S2c)**. Of note, we previously found that fibroblast-specific P2rx4 KO
108 mice had decreased lung fibrosis[13]. Consistent with the importance of P2rx4-dependent IL6 to the fibrotic
109 response after injury, we confirmed that IL6 KO mice were protected from lung fibrosis (**Figure S2d-e**).
110 Furthermore, confirming myeloid cells as one important source of eATP, cell ablative airway liposomal
111 clodronate treatment significantly decreased lung lavage eATP levels (**Figure S2f-h**).

112 ***Fibroblast IL-6 regulates macrophage Arg1, a profibrotic factor***

113 To examine whether paracrine signals referable to P2rx4 signaling in fibroblasts, such as IL-6 expression,
114 might reciprocally regulate macrophage profibrotic responses, we performed differential gene expression
115 analysis from scRNAseq data for WT macrophages cultured with either WT or P2rx4 KO fibroblasts. The
116 top differentially expressed gene was *Arg1*, and its expression was dependent on fibroblast P2rx4
117 expression (**Figure 2a**). We hypothesized that fibroblast-derived IL-6, which was decreased in P2rx4 KO
118 fibroblasts, may regulate macrophage *Arg1* expression as found in other systems [16]. Analysis of ligand-
119 receptor interaction via CellChat[17] and Ingenuity Pathways Analysis confirmed suppression of IL-6
120 signaling in the P2rx4 KO condition (**Figure 2b**). We then confirmed an increase of Arg1 in both cellular
121 lysates and conditioned media of cultured lung macrophages treated with IL-6 (**Figure 2c**). Importantly,
122 treatment with anti-IL6 antibody or IL6 deletion in mice decreased Arg1 protein in the bronchoalveolar
123 lavage fluid following bleomycin injury (**Figure 2d**).

124 Interestingly, analysis of a published scRNAseq time course following bleomycin lung injury[18]
125 showed maximal *Arg1* in cells annotated to be similar to the C2 transitional macrophage compartment
126 we previously demonstrated to localize to the fibrotic niche after injury[4] (**Figure 2e; Figure S3a**). C2 cells
127 not only expressed higher Arg1 but also expressed higher levels of the Fab5 markers that were recently
128 found to be associated with pro-fibrotic macrophages in both mouse and human fibrotic lung and liver

129 datasets[19]. Flow cytometry confirming *Arg1* expression in CD11b+CD64+ macrophages at the 10-day
130 time point, as opposed to monocytes, alveolar macrophages, or dendritic cells (**Figure 3a-b, Figure**
131 **S3b**). Arg1 is often cited as a macrophage marker, but studies of its functional role in fibrosis are limited.
132 Similar to our previous findings for these transitional cells[4], Arg1+ cells were found in proximity to clusters
133 of activated fibroblasts that form after injury (**Figure 3c**). We then treated bleomycin-injured mice with
134 the Arg1 inhibitor CB-1158[20] during the fibrotic period. Importantly, we found that lung fibrosis was
135 significantly decreased and weight recovery improved with Arg1 inhibition (**Figure 3d, Figure S4a**).
136 Taking a genetic approach with macrophage-specific Arg1 homozygous KO mice, we found that lung
137 fibrosis was likewise decreased after injury (**Figure 3e**). To further test the significance of *Arg1*+
138 macrophages, we first performed scRNAseq analysis of aged mice compared to young, given that aging
139 is a major risk factor for the development of lung fibrosis in patients. *Arg1*+ macrophages were increased
140 in bleomycin-injured aged mice at an earlier time point than we observed in young mice—7 days as
141 opposed to 14 days; furthermore, Arg1+ macrophages co-expressed the Fab5 profibrotic macrophage
142 genes[19] (**Figure S4b**). These data suggest a potential predisposition to the fibrotic macrophage profile in
143 aged mice.

144 ***Arg1 regulates availability of ornithine, a pro-fibrotic substrate***

145 To explore the mechanism of Arg1's profibrotic effect, we considered that Arg1 enzymatically converts
146 arginine to urea and ornithine, and that macrophages expressing Arg1 have been found to increase
147 ornithine in the tissue microenvironment[21]. Ornithine can serve as a substrate for the synthesis of
148 proline[22], a major constituent of collagens. Thus, we sought to determine if Arg1+ macrophages supply
149 ornithine as a substrate for collagen production by fibroblasts. First, consistent with a potential for
150 ornithine to drive collagen production, we found that exogenous ornithine increased fibroblast collagen
151 expression at the protein level (**Figure S4c**). Furthermore, in cocultures, Arg1 inhibition with CB-1158, or
152 use of fibroblasts with deletion of IL-6 or P2rx4, decreased collagen expression, whereas ornithine
153 treatment rescued it (**Figure 4a**). We next tested the hypothesis that Arg1-mediated ornithine production
154 was necessary for increasing fibroblast proline content. Consistent with this hypothesis, treatment of

155 cocultures with CB-1158 decreased fibroblast proline (**Figure 4b**). When we treated primary lung
156 fibroblasts in monoculture with $^{13}C_5$-ornithine, we detected an m + 5 mass shift in proline ($^{13}C_5$ proline),
157 consistent with direct conversion of ornithine to proline via the pyrroline 5-carboxylate (P5C) intermediate;
158 glutamine is another source of production of P5C, and glutamine-free conditions, as expected, increased
159 the proportion of $^{13}C_5$ proline further (**Figure S4d**). To test the *in vivo* significance, we treated mice injured
160 with bleomycin with or without ornithine by oral gavage twice daily during the fibrotic phase after injury
161 and found that ornithine treatment significantly increased lung fibrosis (**Figure 4c**). Taken together, these
162 results suggests that macrophage Arg1 drives fibrosis by the production of ornithine, which increases
163 proline content augmenting collagen synthesis.

164 ***Arg1 is expressed in myeloid cells in IPF lung***

165 To address clinical significance, we interrogated ARG1 expression in human lung samples. First, analysis
166 of a published dataset of BAL cell gene expression by microarray[23] confirmed higher expression in IPF
167 compared to healthy controls (**Figure S5a**). We then confirmed ARG1 expression by
168 immunofluorescence in IPF lung explants acquired at the time of clinical transplantation, whereas less
169 ARG1 was expressed in deceased donor lungs not known to have lung disease (**Figure 5a**). To
170 determine cell type, we performed multiplexed ion beam imaging (MIBI) using an extensive panel of
171 myeloid and lymphoid markers. We found that ARG1+ cells were CD11B+ and CD16+, consistent with
172 myeloid lineage, and were also positive for the granulocyte marker CD66B. Interestingly, the macrophage
173 markers CD163 and CD68 were not expressed (**Figure 5b**). To confirm, we performed 10x Xenium
174 spatial transcriptomic analysis of IPF samples and found ARG1+ cells had higher expression compared
175 to ARG1- cells for CD11B (*ITGAM*), CD66B (*CEACAM8*) but not *CD163* or *CD68* (**Figure S5b**). Taken
176 together, these data suggest that, in IPF, ARG1 is expressed in myeloid cells of the granulocytic lineage.

177 To test whether ARG1+ cells localize in proximity to IL-6+ cells, we analyzed the Xenium data of
178 the IPF samples. We defined a proximity statistic that allowed us to quantitatively compare the
179 probabilities of detecting an IL6+ fibroblast versus an IL6- fibroblast within a given distance from an
180 ARG1+ cell (**Methods**). Interestingly, we found that ARG1+ cells were more likely to be close to IL6+

181 fibroblasts compared to IL6- fibroblasts, up to and including a distance of 100μm, a distance that could
182 be considered consistent with paracrine effects (**Figure 5c**). For functional testing, we prepared
183 precision-cut lung slices and treated them with CB-1158 or the IL6RA-blocking antibody tocilizumab for
184 24 hours. Collagen expression was decreased with both treatments compared to untreated slices,
185 suggesting inhibition of new collagen synthesis (**Figure 5d**). Taken together, these data indicate ARG1
186 is a contributor to the pathologic accumulation of collagen in IPF.
187

188 **Discussion**

189 Our findings reveal a novel paracrine communication network between macrophages and fibroblasts that
190 regulates fibrosis. A key advance was the discovery of a profibrotic function of inflammatory fibroblasts.
191 Specifically, these cells expressed IL-6, which was necessary for induction of Arg1 resulting in production
192 of the pro-fibrotic amino acid ornithine. Our coculture experiments identified macrophage-derived eATP
193 as the initiator of P2rx4-dependent IL-6 expression in fibroblasts. eATP is a damage- and inflammation-
194 associated molecule that has been implicated in fibroblast IL-6 expression[24, 25], and we previously found
195 that fibroblast-specific P2rx4 KO mice had decreased lung fibrosis after injury[13]. Here we confirmed that
196 IL-6 induced macrophage Arg1[26, 27, 28] and then advanced understanding of Arg1 function by
197 demonstrating the key profibrotic role of its reaction product ornithine as a substrate for collagen
198 production.

199 Mechanistically, we define a novel metabolic pathway wherein ARG1-dependent production of
200 ornithine directly increased collagen expression. Our metabolomic studies indicate conversion of
201 ornithine to proline, a key substrate for collagen synthesis. However, we note that ornithine conversion
202 to polyamines with profibrotic potential remains a further possibility not yet addressed by our work.
203 Furthermore, ARG2 is a second arginase that could also contribute to ornithine loading of fibroblasts.
204 Future studies should focus on how both arginases are regulated across the temporal phases of fibrosis,
205 including both initiation of fibrosis and its progression in cases leading to organ failure.

206 This work addresses the limited understanding of cell-to-cell signals that underlie tissue
207 remodeling in the fibrotic niche. In previous studies, single-cell profiling of tissues in the setting of fibrosis
208 led to the discovery of markers for both scar-associated macrophages and multiple subtypes of
209 fibroblasts[1, 2, 29]. However, crosstalk mechanisms between the macrophages and fibroblasts in tissues
210 have not been extensively studied, with current knowledge derived mostly from *in vitro* modeling[30]. Our
211 work maps interactome analysis from cultured cells onto the relevant tissular context, enhancing
212 understanding of cell-to-cell communication *in vivo*, an unmet need in the field[29]. Furthermore,
213 inflammatory fibroblasts have come to attention as present in both infectious[31] and fibrotic[2, 3] models;
214 their function in fibrosis is further elucidated by our discovery of macrophage eATP-induced IL-6 and its
215 reciprocal induction of Arg1 in macrophages, for pro-fibrotic ornithine loading of fibroblasts.

216 Interestingly, in schistosomiasis-induced fibrosis models, Arg1 deletion in macrophages led to an
217 increase in type 2 inflammation, and consequently increased fibrosis, because of an accumulation of
218 arginine, which supports CD4 T cell proliferation[32]. However, in IPF and in murine bleomycin-induced
219 pulmonary fibrosis, type 2 inflammation does not appear to be an important driver of fibrosis. Inhibition of
220 type 2 inflammation with dual IL-4 and IL-13 blockade failed to show efficacy in a clinical trial of IPF[33].
221 Furthermore, in the bleomycin-induced sterile injury model that we have used, the onset of type 2
222 inflammation is later than the period when significant collagen deposition has already occurred and is
223 therefore less relevant to fibrogenesis[34]. Although inhibition of Arg1 might be contraindicated in patients
224 with schistosomiasis, our data provide a strong rationale for further investigation of the potential role of
225 Arg1 inhibition for treatment of IPF.

226 Previous studies have reported the expression of ARG1 in myeloid cells from lung fibrosis
227 patients[35, 36]. Importantly, we confirmed functional relevance in human lung fibrosis by showing that
228 arginase inhibition decreased lung fibrosis in precision-cut lung slices from IPF. Furthermore, our
229 proximity analysis for ARG1+ cells and IL-6+ fibroblasts suggests that induction of ARG1 in human fibrotic
230 lung may be dependent on IL-6, similar to our studies in mice. However, our multiparameter imaging with
231 MIBI provided a refined view of marker expression of these cells and showed that ARG1+ cells are likely

232 similar to granulocytes previously identified in human tumors[37, 38, 39]. Gene expression is well known to
233 differ across species by immune compartment[40], and the case of Arg1 provides an important instance: In
234 mice, Arg1 was expressed in profibrotic, transitional macrophages in fibrotic areas of mouse lung,
235 whereas in human lung fibrosis, ARG1+ cells expressed CD11B and CD66B but not other macrophage
236 markers, consistent with granulocytic lineage.
237

238 **Methods**

239 ***Human lung tissues***

240 The studies described in this paper were conducted according to the principles of the Declaration of
241 Helsinki. IPF lung samples were obtained as explants at the time of lung transplantation. Written,
242 informed consent was obtained from all subjects, and the study was approved by the University of San
243 Francisco, California institutional review board. Deceased donor-control lungs not known to have lung
244 disease were made available by Donor Network West. Because these samples were acquired from
245 deceased individuals the study is not considered human subjects research as per UCSF and NIH policy.

246 ***Mice***

247 Pdgfrb-Cre[41], Lysm-Cre [42], P2rx4 floxed[43], Arg1 floxed[44], Col1a1-EGFP[45], Arg1-RFP-CreERT2[46], and
248 Arg1-YFP[47] mice were available to the investigative team, and IL-6 KO[48], WT, and R26-LSLS-TdTomato
249 mice were obtained from JAX. Col1a1-GFP mice were obtained from David Brenner[45]. All mice were
250 maintained on a C57BL/6 background and were maintained in specific pathogen-free animal barrier
251 facility at the University of California, San Francisco. All experiments were performed on 6-8 weeks old,
252 sex-matched mice, or in the case of aged mice, 24-month-old, sex-matched mice, and were performed
253 in accordance with approved protocols by the University of California, San Francisco Institutional Animal
254 Care and Use Committee.

255 ***Mouse lung injury, cell isolation, and macrophage-fibroblast coculture***

256 For lung injury, mice anesthetized with isoflurane were instilled intratracheally with bleomycin (Fresenius,
257 3U/Kg), and lungs were isolated after 7 days after injury. In the case of Arg1 inhibition, bleomycin-injured

258 mice were treated daily from day 9 to day 15 post-injury with 100 mg/kg CB-1158 (Numidargistat
259 dihydrochloride) dissolved in water, by oral gavage. In the case of ornithine treatment, mice were treated
260 daily by gavage with ornithine 2 mg/kg dissolved in 100 μL of water. For the creation of single-cell
261 suspensions, lungs were harvested from euthanized mice and minced with scissors, the tissue was
262 resuspended in RPMI with 0.2% Collagenase (10103586001, Roche), 2000 U/ml DNase I (4716728001,
263 Roche) and 0.1 mg/ml Dispase II (4942078001, Sigma). The suspension was incubated for 1 hour at
264 37°C and passed through a 70 μm filter (130-110-916, MACS SmartStrainers) to obtain single cells. The
265 cells were washed twice with 1X PBS pH 7.4 (10010023, Gibco). For macrophage isolation, a total of $10^7$
266 cells were resuspended in 80μl PBS buffer supplemented with 0.5% BSA (0332, VWR Life Science) and
267 2mM EDTA (E57040, Research Products International). 20μl CD11b microbeads were used per $10^7$ cells.
268 Macrophages were obtained by positive selection by binding to CD11b microbeads and passing through
269 MACS columns (130-049-601, Miltenyi Biotech). Isolated $CD11b^+$ macrophages were cultured in DMEM
270 supplemented with 10% FBS, 1% penicillin-streptomycin, and 20 ng/ml M-CSF (315-02, Peprotech) for
271 2 days. Primary mouse lung fibroblasts were freshly isolated after magnetic bead-based negative
272 selection of epithelial cells (118204, Biotin anti-mouse CD326 Epcam, Clone: G8.8, BioLegend),
273 endothelial cells (102404, Biotin anti-mouse CD31, clone: 390), immune cells (103104, Biotin anti-mouse
274 CD45, clone: 30-F11, BioLegend), pericytes and smooth muscle cells (134716, Biotin anti-mouse CD146,
275 clone: ME-9F1, BioLegend), and red blood cells (116204, Biotin anti-mouse Ter119, clone: TER-119,
276 BioLegend) with biotinylated antibodies and Dynabeads (MyOne Streptavidin T1, 65601, Thermo Fisher
277 Scientific) as previously described[2]. Fibroblasts were cultured for 5 days prior to trypsinization and
278 addition to macrophages for coculture at a 1:1 ratio in DMEM complete media for 5 further days.

279 ***Human lung cell isolation and macrophage-fibroblast coculture***

280 Human lung tissue from deceased donors not used for transplant was resected and minced in Hanks'
281 Balanced Salt Solution (HBSS) buffer supplemented with 0.2% Collagenase (10103586001, Roche),
282 2000 U/ml DNase I (4716728001, Roche) and 0.1 mg/ml Dispase II (4942078001, Sigma), 1% Penicillin-

283 streptomycin for 1.5 hours at 37°C and 5% CO2. 1X Amphotericin B (15290026, Gibco) was added to
284 the dissociation solution for 30 min. Digested lung tissue was lysed further with a MACS tissue dissociator
285 (gentleMACS Dissociator, Miltenyi Biotec) using gentleMACS C tubes (130-093-237, Miltenyi Biotec) at
286 mLUNG-01 setting. The suspension was then passed through a 70 μm filter to obtain single cells. Cells
287 were resuspended in PBS with 0.5% BSA and 2mM EDTA. Macrophages were incubated with CD11b
288 microbeads and loaded on MACS columns. After washing the cell fraction of unlabeled cells, CD11b+
289 cells were eluted and cultured in DMEM supplemented 10% FBS (10082147 Gibco), 1% penicillin-
290 streptomycin (1670249, MP Biomedicals), and 50 ng/ml human M-CSF (300-25, Peprotech) for 2 days.
291 For the negative selection of human fibroblasts, the following antibodies were used at a 1:200 ratio:
292 epithelial cells (324216, Biotin anti-human Epcam, clone:9C4, BioLegend), endothelial cells (13-0319-
293 82, Biotin anti-human CD31, clone: WM-59, Invitrogen), immune cells (368534, Biotin anti-human CD45,
294 clone: 2D1, BioLegend), pericytes and smooth muscle ( 361036, Biotin anti-human CD146, clone:
295 P1H12, BioLegend). Fibroblasts were added directly to the cultured macrophages, and the cells were
296 cocultured in DMEM supplemented with 10% serum, 1% penicillin-streptomycin, and 1% amphotericin B
297 for a total of 5 days.

298 ***Flow cytometry***

299 *Cocultured cells:* Cocultures were trypsinized with 0.25% trypsin and resuspended in 1X PBS with 0.5%
300 BSA and 2mM EDTA. Single-cell suspensions were pre-stained with Fc blocker for 10 min in ice followed
301 by staining at 1:300 with anti-CD64 (139304, PE anti-mouse CD64, clone:X54-5/7.1, BioLegend) and
302 anti-Pdgfra (25-1401-82, PE-Cy7, anti-mouse CD140a, clone: APA5, Invitrogen) antibodies for 40 min.
303 DAPI was used to distinguish dead cells.

304 *Mouse lung cell suspensions (for clodronate macrophage depletion experiments):* Single cell
305 suspensions from digested mice lungs were incubated with ghost dye 516 (13-0867-T100, TONBO)
306 1:300 for 30min in ice followed by washing with staining buffer consisting of 1% EDTA and 1% serum in
307 PBS. Cells were stained with anti-CD64 (139304, PE anti-mouse CD64, clone:X54-5/7.1, BioLegend)

308 and anti-CD11b (25-0112-81, PE-Cy7, clone:M1/70, eBioscience) antibodies for 40 min at 4°C protected
309 from light. Cells were washed with staining buffer and resuspended in 100μl staining buffer and 100μl IC
310 fixation buffer. Samples were kept in dark at 4°C overnight followed by resuspending in 300μl staining
311 buffer. Data was acquired using Fortessa (BD Bioscience) and analyzed using FlowJo software.
312 *Mouse lung cell suspension (for experiments with Arg1-YFP mice):* Whole lung single cell suspensions
313 were prepared by harvesting lung lobes into 5 ml HBSS with 40μl Liberase Tm (0.1 U/ml, Roche, Cat#
314 5401127001) and 20μl DNAse 1 (10mg/ml, Roche, Cat# 10104159001), followed by automated tissue
315 dissociation (GentleMacs; Miltenyi Biotec) and tissue digestion for 30 min at 37°C on a shaker. Digested
316 samples were processed on the GentleMacs using the "lung2" program, passed through 70μm filters,
317 and washed, followed by red blood cell lysis and final suspension in FACS buffer. Cells were counted
318 using a NucleoCounter (Chemometic). All samples were stained in 96-well V-bottom plates. Single cell
319 samples were first incubated with antibodies to surface antigens for 30 min at 4°C in 50μl staining volume.
320 Flow cytometry was performed on BD LSRFortessa X-20. Fluorochrome compensation was performed
321 with single-stained UltraComp eBeads (Invitrogen, Cat# 01-2222-42). Samples were FSC-A/SSC-A
322 gated to exclude debris, followed by FSC-H/FSC-A gating to select single cells and Draq7 viability dye
323 (Biolegend) to exclude dead cells. Early transitional macrophages (TMs) were identified as $CD19^-$, $Ly6G^-$
324 , $NK1.1^-$, Siglec-$F^-$, $CD11b^+$,$CCR2^+$ and $CD64^+$. Late TMs were identified as $CD19^-$, $Ly6G^-$, $NK1.1^-$, Siglec-
325 $F^-$, $CD11b^+$, $CCR2^-$ and $CD64^+$. GR1 MDSC were identified as $CD19^-$, $Ly6G^+$, $CD64^-$ and $CD11c^+$.
326 Arginase1-positive cells were identified by the presence of eYFP. Data were analyzed using FlowJo
327 software (TreeStar, USA) and compiled using Prism (GraphPad Software). Monoclonal antibodies used
328 were: anti-CD45 (30-F11, Biolegend), anti-CD11b (M1/70, Biolegend), anti-CD11c (N418, Biolegend),
329 anti-NK1.1 (PK136, Biolegend), anti-CD19 (6D5, Biolegend), anti-T1/ST2 (DJ8, BD BioSciences), anti-
330 MerTK (DS5MMER, eBiosciences), anti-CD64 (X54-5/7, eBiosciences), anti-Ly6C (HK1.4), anti-Ly6G
331 (1A8, Biolegend), anti-SiglecF (E50-2440), and anti-I-A/I-E (MHCII) (M5/114.15.2, Biolegend), anti-CCR2
332 (475301, BD BioSciences).

333 ***Quantitative Real-Time PCR analysis***

334 Macrophages or fibroblasts were lysed in 300μl TRIzol reagent (10296010, Ambion life technologies) to
335 obtained RNA. 600 ng of RNA per sample was used to prepare cDNA using iScript reverse transcriptase
336 supermix (Bio-Rad, 1708841). qPCR was performed for the target genes using SYBR Green super mix
337 (Applied Biosystems, 4309155). Gene expression was normalized to Gapdh for analysis of mouse
338 transcripts or 18S rRNA for human.

339 Mouse *Gapdh* Forward: AGTATGACTCCACTCACGGCAA

340 Mouse *Gapdh* Reverse: TCTCGCTCCTGGAAGATGGT

341 Mouse *IL6* Forward: CCAAGAGGTGAGTGCTTCCC

342 Mouse *IL6* Reverse: CTGTTGTTCAGACTCTCTCCCT

343 Human 18S rRNA Forward: GTAACCCGTTGAACCCCATT

344 Human 18S rRNA Reverse: CCATCCAATCGGTAGTAGCG

345 Human IL6 Forward: ACTCACCTCTTCAGAACGAATTG

346 Human IL6 Reverse: CCATCTTTGGAAGGTTCAGGTTG

347

348 ***ATP measurement***

349 For ATP measurement, 1 mL of mouse lung lavage was collected in 1X PBS containing 100μM ATPase
350 inhibitor. ATP measurement was performed immediately by measuring bioluminescence using Biotek H1
351 plate reader as described in the manufacturer's protocol (A22066, ATP determination Kit, ThermoFisher
352 Scientific). Briefly, an assay solution was prepared by mixing a working concentration of 10μM
353 dithiothreitol, 0.2mM D- luciferase, 7.5 μg/ml firefly luciferase in 1X reaction buffer diluted with distilled
354 water. The reaction was kept in ice and protected from light. 10 μl of sample was mixed with 90 μl of
355 assay solution, and light emission was measured at 560 nm using a Biotek plate reader.

356 ***Macrophage depletion***

357 Mice were treated 6 days after bleomycin lung injury with 100μl of 18.4 mM liposomal-clodronate (CLD-
358 8909, Encapsula NanoSciences) by oral aspiration. Mice were kept under observation for 24hrs. These
359 mice were euthanized on day 7, and bronchoalveolar lavage fluid was collected in PBS containing 100μM
360 ATPase inhibitor, and lung cell suspensions were prepared for flow cytometry.

361 ***siRNA Knockdown***

362 Healthy human fibroblasts were treated with 5μM siRNA (Dharmacon, D-001810-01-05 ON-TARGET
363 plus No-targeting siRNA) control or (Dharmacon, L-006285-00-0010 ON-TARGET plus Human P2RX4
364 SMARTpool) using DharmaFECT in serum-free media for 12 hours, followed by supplementing with
365 DMEM with 10% serum. Cells were incubated for an additional 48 hours. Treated cells were harvested
366 for either RNA isolated or stimulated with 100μM ATPγS for 12 hours and culture supernatant was
367 collected for Human IL6 ELISA assay.

368 ***IL-6 ELISA***

369 *For Mouse*: Bronchoalveolar lavage fluid or conditioned culture media were collected for measurement
370 of IL-6 with a Duoset ELISA kit (R&D Systems, DY406-05).

371 *For Human*: Culture supernatant was collected and IL6 was measured using Duoset ELISA kit (R &D
372 system, DT206-05). Briefly, the capture antibody was coated overnight in a 96-well plate at room
373 temperature. Wells were aspirated and washed in ELISA wash buffer and blocked by adding reagent
374 diluent consisting of 1% BSA in PBS. After 1 hour of room temperature incubation, wells were again
375 washed with wash buffer and samples or standards were added and incubated for 2 hours at room
376 temperature. Detection antibody was used along with streptavidin-HRP and substrate solution. The
377 reaction was stopped with stop solution, and optical density was measured using a microplate reader at
378 450 nm.

379 ***Mouse Arginase 1 ELISA***

380 Arginase 1 levels were measured from conditioned media or from bronchoalveolar lavage, using Mouse
381 Arginase 1 ELISA Kit (ab269541, Abcam) based on the manufacturer's protocol. Briefly, CD11b+ mouse

382 lung cells were seeded in 12-well dishes for 2 days in DMEM supplemented with M-Csf (315-02,
383 Peprotech). Cells were exposed to murine IL-6 for 72 hours, and culture supernatant and cell lysate were
384 then collected. For in vivo experiments, bleomycin-injured mice received intraperitoneal treatment with a
385 150 µg/kg dose of anti-IL6 antibody (MP5-20F3, BioCell) or IgG control (MAB005, R & D systems) on
386 days 6, 9, and 12, followed by bronchoalveolar lavage isolation on day 14 from the indicated groups. For
387 the ELISA, subsequently, 50 µl of undiluted samples were added to each well, along with a 50 µl antibody
388 cocktail comprising capture antibody and detection antibody dissolved in antibody diluent. Plates were
389 incubated for 1 hour at room temperature. Wells were washed thrice with wash buffer and incubated with
390 100 µl Tetramethylbenzidine (TMB) substrate for 15 min. The reaction was stopped using 100µl stop
391 solution, and OD was measured at 450nm.

392 ***Histology and Immunofluorescence imaging***

393 *Mouse lung:* Arg1-RFP-creERT2 /Rosa26-LSL-TdTomato/Col1a1-EGFP mice were injured for 14 days.
394 Lungs from uninjured and injured mice were fixed in 4% formaldehyde at 4$^{o}$C for 4 hours, then washed
395 and submerged in 30% sucrose solution overnight at 4$^{o}$C. Next, the tissue was incubated in 1:1 solution
396 of 30% sucrose and OCT (4585, OCT) overnight followed by changing to OCT for 2 hours, and then a
397 tissue block was frozen after embedding in OCT. 5 µm sections were cut from OCT-embedded tissue.
398 For immunofluorescence imaging, slides with sections were washed with PBS and mounted on antifade
399 DAPI mounting media and imaged using a Leica inverted widefield confocal laser scanning microscope
400 at BIDC, UCSF.

401 For Sirius Red imaging, sections prepared from mouse lungs frozen in OCT were stained with
402 Sirius Red (0.1% Sirius Red in saturated picric acid, Electron Microscopy Sciences, 26357-02) for 60 min
403 followed by a 2-min 0.01 N HCl wash, rinsed in 70% ethanol, and air-dried overnight before imaging.
404 Images were acquired using a bright-field microscope (Zeiss Axio scan.Z1). The images were quantified
405 using Qupath image analysis software using the artificial neural network pixel classifier function[49], with
406 software training based on user-defined fibrotic regions in a single image.

407 *Human lung:* 5 μm thick sections from patient FFPE blocks were collected for IHC staining. Slides were
408 stained using Opal Manual IHC kit (PerkinElmer). After deparaffinization, antigen retrieval was performed
409 in AR buffer for 45 sec at 100% power followed by 15 min at 20% power. After blocking slides were
410 incubated with Primary antibodies ARG1 (CST) overnight at 4C. Polymer HRP was introduced to slides
411 for 10 min, followed by signal amplification using Opal570 for 10 min at room temperature. The slides
412 were then counterstained with DAPI mounting media and scanned using with a 10x and 40x objective of
413 Leica inverted widefield microscope.

414 ***Western blot***

415 Precision cut lung slices were obtained from human IPF tissue sections. Briefly, IPF tissue was injected
416 with 2% low melting agarose (50111, Lonza) and then submerged in ice-cold PBS to allow solidification
417 of agarose. 400 μm lung slices was generated using Compresstome (VF-310-OZ, Precisionary
418 Instruments). Slices were kept in complete DMEM media for 2 hours to allow the release of agarose
419 followed by changing to fresh complete DMEM. Lung slices were treated with 50 μM CB1158 or 10 μg/ml
420 Tocilizumab for 24 hours. After incubation slices were minced using a tissue homogenizer. Cells were
421 lysed in Pierce RIPA buffer (Thermo Fisher Scientific, 89901) with protease inhibitor cocktail (Thermo
422 Fisher Scientific, 1861278). 10 μg of protein was run on 10% sodium dodecyl sulfate-polyacrylamide gel
423 electrophoresis (Bio-rad, 4561034) and transferred to a PVDF membrane (Thermo Fisher Scientific,
424 88520). The membrane was incubated with 1:1000 Col1a1(#720265, Cell Signaling Technology)
425 overnight at 4°C. Blots were washed in 1XTBST and incubated with peroxidase-conjugated goat anti-
426 rabbit (1:20,000, Anaspec, AS28177) for 4 hr at 4°C. These blots were developed using SuperSignal
427 West Pico Chemiluminescent substrate (Thermo Fisher Scientific, 34080) in ChemiDoc XRS+ gel
428 imaging system (Bio-rad). Quantification of bands was done using ImageJ.

429 ***Hydroxyproline assay***

430 Mice were euthanized and lungs were excised and snap-frozen. Isolated lung samples were
431 homogenized and incubated with 50% trichloroacetic acid (T6399, Sigma) on ice for 20 min. Samples

432 were then incubated in 12N HCL (A144, Fisher) overnight at 110°C. Dried pellets were reconstituted in
433 distilled water with constant shaking for 2 hours at room temperature. Samples were then mixed with
434 1.4% Chloramine T (Sigma, 85739) and 0.5 M sodium acetate (Sigma, 241245) in 10% 2-propanol
435 (Fisher, A416) and incubated with Ehrlich's solution (Sigma, 03891) for 15 min at 65°C. Absorbance was
436 quantified at 550 nm, and concentration was calculated using a standard curve of commercial
437 hydroxyproline (Sigma, H5534).

438 ***scRNAseq library preparation and sequencing***

439 PIPseq T2 3' Single Cell RNA Kit (v3.0 – cultured cells, v4.0 – directly sequenced cells) was used for
440 pre-templated instant partitioning (PIP) to capture single-cell mRNA transcripts with PIP beads according
441 to manufacturer's protocol (Fluent Biosciences, FB0001026). In the case of directly sequenced cells, 7
442 days after bleomycin injury, cells were isolated by the isolation procedure described above for scRNAseq
443 workflow. In the case of cocultures, 7 days after bleomycin lung injury, mice were euthanized and lungs
444 were harvested followed by cell isolation as above. After 5 days of coculture, single cell suspension of
445 cells was obtained by trypsinization followed by washing in 1X PBS.

446 Cells were washed in ice-cold PIPseq Cell Suspension Buffer (Fluent Biosciences, FB0002440).
447 Cells were counted and stained with Trypan blue to confirm >90% viability. Single-cell library preparation
448 was performed using the manufacturer-recommended default protocol and settings. The sequencing
449 libraries were submitted to UCSF Center for Advanced Technology (Novaseq X) or Novogene (Novaseq
450 6000) for sequencing. The demultiplexed FASTQ files were aligned to mouse genome (mm10) using
451 PIPseeker 1.0.0 (Fluent Biosciences). After sequence alignment, we observed around 50% of input cells
452 being called when PIPseeker sensitivity level was set to 3, which was near the inflection point of the
453 barcode rank plot. The original FASTQ files, the quality reports, and the expression matrix outputs of
454 PIPseeker have been deposited in Gene Expression Omnibus (GEO).

455 ***scRNAseq Data Analysis***

456 The Seurat – Guided Clustering Tutorial (March 27, 2023) was followed to convert our expression
457 matrixes into Seurat objects (Seurat version 4.3.0)[50]. For quality control, we removed the cells with less

458 than 200 genes or more than 10,000 genes and larger than 5% mitochondrial content. Seurat objects
459 were integrated following Seurat's Introduction to scRNAseq Integration (March 27, 2023), selecting the
460 top 2,000 variable features as integration anchors. Cell doublets were removed with the package
461 DoubletFinder (2.0.3) [51]. Following Seurat – Guided Clustering Tutorial (March 27, 2023), we selected
462 the top 2000 highly variable genes to obtain the cell UMAP coordinates and group the cells into clusters
463 with a sensitivity of 0.5[50]. Cell types were annotated using the SingleR package 1.10.04[4] using the
464 ImmGen database[52] as reference. The Gene Set Enrichment Analysis (GSEA) was performed using the
465 package enrichR 3.1[53] (FDR<0.05), with gene ontology data taken from the database
466 "GO_Biological_Process_2021"[54]. Cell communication pathways analysis was performed using the
467 package CellChat (1.6.1)[17]. Upstream regulator prediction was done using the Ingenuity Pathway
468 Analysis software (Qiagen)[55]. Differentially expressed genes for macrophages with $p < 0.05$ and average
469 log2 fold change > 0.75 were used for analysis. Analysis results with $p < 0.05$ were considered significant.

470 ***Multiplexed Ion Beam Imaging and Analysis (MIBI)***

471 *Slide Preparation:* Serial 5 um FFPE sections were cut onto one glass and one gold slide. Both slides
472 were baked at 70* Celsius overnight and deparaffinized in three washes of fresh Xylene and rehydrated
473 in EtOH (2X 100% EtOH, 2X 90% EtOH, 1X 80% EtOH, 1X 70% EtOH) and distilled water (2X) washes.
474 Washes were performed in (include wash machine specs). An antigen retrieval slide chamber was
475 prepared by diluting 10X Tris with EDTA antigen retrieval buffer 1:10 in diH2O (Reagent Details). The
476 prepared slide chamber was added to a PT Module (add specs) filled with PBS and preheated to 75ºC.
477 The rehydrated slides were run in the preheated PT module at 97ºC for 40 minutes, then cooled to 65ºC
478 in the PT module. The prepared slide chamber was then removed from the PT module and cooled at RT
479 for 30 minutes. Slides were washed 2X in 1X TBS-Tween (Add reagent details).

480 *Glass Slide IHC:* Tissues were encircled by PAP pen boarders and blocked with 5% donkey serum
481 (reagent details) diluted in TBS IHC wash buffer (reagent details) for 1 hour at RT in a moisture chamber.
482 Wash buffer was aspirated from the slide, and Arginase-1 primary antibody (Ionpath Cat#: 715001) was
483 stained overnight at 4ºC overnight in the moisture chamber. The following day, primary antibody was

484 aspirated, and slides were washed twice with 1X TBS-T for 5 minutes, blocked with 3% peroxide buffer
485 for 15 minutes at RT, and washed again twice with 1X TBS-T for 5 minutes each wash before incubation
486 with anti-rabbit secondary antibody (reagent details) for 1 hour at RT. Slides were washed twice with 1X
487 TBS-T for 5 minutes before visualization with 100uL DAB (reagent details) for 5 minutes at RT. DAB
488 reaction was stopped by tapping waste into contained waste bin, and then washing the slide into a slide
489 chamber filled with diH2O 3X for 30 seconds each wash. The slide was then stained with Hematoxylin
490 for 1 minute at RT, and washed with tap water 2X for 30 seconds. The slide was then dehydrated by
491 washing in EtOH (1X 70% EtOH, 1X 80% EtOH, 2X 95% EtOH, 2X 100% EtOH), and Xylene (2X) before
492 cover slipping.
493 *Gold Slide Staining:* Gold slides were transferred the Sequenza Immunostaining Center Staining System
494 (Electron Microscopy Sciences, Hatfield, PA). Endogenous biotin-binding proteins with blocked with
495 (Avidin/biotin-blocking reagents) for 30 minutes at room temperature. 5% donkey serum was added to
496 the top of the chamber to wash out the avidin blocking reagents and block additional non-specific antibody
497 binding sites for 1 hour at RT. Primary and Secondary antibodies panels were assembled with appropriate
498 volumes of each titrated antibody and a final concentration of 0.05M EDTA. The complete cocktails were
499 filtered through a pre-wet 0.1 um Ultragree MC Spin Filter, (cat#) then the Primary Antibody cocktail
500 (**Table S2**) was added to the Sequenza top chamber and incubated overnight at 4ºC. The Secondary
501 antibody cocktail was stored at 4ºC. The following day, the slides were washed by adding 1X TBS-T to
502 the Sequenza chamber 2X before adding the Secondary Antibody cocktail to the Sequenza chamber for
503 1 hour at RT. Gold slides were removed from the Sequenza chamber and washed 3X with 1X TBS-T for
504 5 minutes each wash, 1X with filtered 2% Glutaraldehyde for 5 minutes, 3X with filtered 1X Tris pH 8.5,
505 2X with filtered diH2O, 1X with 70% EtOH, 1X with 80% EtOH, 2X with 90% EtOH, and 2X with 100%
506 EtOH. Slides were allowed to dry at RT for 10 minutes before being stored in a vacuum chamber (Cat#)
507 before MIBIscope analysis.
508 *Image Acquisition and Processing:* Gold slides were loaded into the MIBIscope (Ionpath, Menlo Park,
509 CA) and FOVs were selected by matching tissue topography to ROIs with Arginase-1+ Staining from the

510 serial IHC glass slide. FOVs were acquired at Fine resolution, with a dwell time of 1 second at a resolution
511 of 0.39 um per pixel. Image QC was performed by following the Angelo Lab toffy pipeline
512 (https://github.com/angelolab/toffy). Analysis was performed by following the Angelo Lab ark pipeline
513 (https://github.com/angelolab/ark-analysis).

514 ***Spatial Transcriptomics (10x Xenium)***

515 FFPE preserved sections of lung tissue were prepared for spatial transcriptomics imaging on the Xenium
516 platform by following 10x Genomics protocols CG000582 Rev E and CG000584 Rev A. Briefly, protocol
517 CG000582 prepares the slides for the imaging run by first hybridizing the probe panel of choice. Here,
518 the standard human lung panel available from 10x Genomics (Cat #1000601) was supplemented with a
519 custom panel specific for lung disease states, including pulmonary fibrosis (**Table S3**). Following probe
520 hybridization, annealed probes are ligated together to create circular fragments, then circularized probes
521 are amplified with a rolling circle PCR. After rolling circle amplification, slides are DAPI stained for nuclei
522 then placed in the Xenium Analyzer with run reagents following CG000584. The gene panel is uploaded
523 to the Xenium Analyzer and a primary image is take of the slides. All areas with visible tissue are selected
524 for imaging and the imaging run is started. The Xenium processes imaging data during the run, identified
525 cell boundaries and outputting image files along with cell by transcript by location matrices for further
526 downstream analysis by Seurat 10x Xenium protocol.

527 *Proximity Analysis of ARG1+ cells and IL6+ CTHRC1+ cells:* The output files of Xenium Analyzer were
528 converted to an AnnData object that contained the cell centroid coordinates and raw transcript counts. A
529 filter of 10 counts per cell and 5 cells per gene was applied to filter out low-quality cells and sparsely
530 detected genes. Counts were normalized to 1e4 and log-transformed. Cells were then grouped into one
531 of the following four categories: ARG1+, IL6+ CTHRC1+, IL6- CTHRC1+, or other, with positive
532 expression of a marker defined as having non-zero counts.

533 *Co-occurrence probability ratio:* The 'Analyze Xenium data' tutorial in Squidpy (version 1.5.0)[56] was
534 followed to compute the co-occurrence probability ratio of ARG1+ and IL6+CTHRC1+ cells, IL6-
535 CTHRC1+ cells, or other cells not bearing these profiles. We performed 50% random subsampling of the

536 data 5 times to compute the statistic and generate confidence intervals bounded by the minimum and
537 maximum probability ratio generated by the subsamples. The co-occurrence probability ratio was
538 computed every 50µm within a range of 250µm. Using the implementation in the 1.5.0 release of Squidpy,
539 for each radial distance, the ratio of cells belonging to category exp (exp being any of the four categories
540 of markers above, ie ARG1+, IL6+ CTHRC1+, IL6-CTHRC1+, or other cells not bearing these profiles)
541 out of all cells within the given distance of an ARG1+ cell was averaged across all ARG1+ cells to
542 compute the conditional probability in the numerator P(exp | ARG1+), while the denominator P(exp) was
543 computed similarly but averaging probabilities that were computed by centering around every cell in the
544 sample. Previous releases of Squidpy implemented a version of this test in the function gr.co_occurrence
545 that used discrete interval bins (only including cells within two consecutive choices of radial distances).
546 We chose to use inclusive intervals (including all cells within a given radial distance) for a more robust
547 calculation of the co-occurrence probability ratio. We implemented our method into the codebase of
548 Squidpy, with the help of Squidpy's authors, and it is now the default implementation of the function
549 gr.co_occurrence, starting in release 1.5.0.

550 ***Analysis of published datasets***

551 Time series of single-cell data after bleomycin lung injury were obtained from Tsukui et al[3] and Strunz et
552 al [18]. These samples were processed and merged with Seurat (4.3.0) using the function SCTransform to
553 correct for batch effects and annotated with SingleR 1.10.044 using the ImmGen database as reference.
554 We subsetted the macrophages from GSE141259[18] repository and annotated by applying SingleR using
555 as reference the macrophage subtypes (C1, C2, C3) defined by Aran et al[4]. Microarray RNA data from
556 bronchoalveolar cells of healthy individuals and IPF patients was extracted from the GPL14550 dataset
557 within the GSE70867[23] repository. The differentially expressed genes between IPF and healthy samples
558 were obtained by following the R workflow provided by the NCBI GEO2R platform using GEOquery
559 (2.66.0) and limma (3.54.2) packages.

560 ***LC-MS metabolomics and $^{13}$C-flux***

561 Primary murine lung macrophages and fibroblasts were cocultured, or fibroblasts were cultured alone,
562 as above, for 24 hours with or without 1mM $^{13}C_5$-ornithine (Cambridge Isotope Laboratories, CLM-4724-
563 H-PK) or 1 mM CB-1158. Cell extracts were used to calculate protein equivalents by resuspension in 0.2
564 M NaOH, heated to 95 °C for 25 min, and determined via BCA (Pierce, 23225). Dried metabolites were
565 resuspended in 50% ACN:water and 1/10th of the volume was loaded onto a Luna 3 um NH2 100A (150
566 × 2.0 mm) column (Phenomenex). The chromatographic separation was performed on a Vanquish Flex
567 (Thermo Scientific) with mobile phases A (5 mM $NH_4AcO$ pH 9.9) and B (ACN) and a flow rate of 200
568 µL/min. A linear gradient from 15% A to 95% A over 18 min was followed by 9 min isocratic flow at 95%
569 A and reequilibration to 15% A. Metabolites were detected with a Thermo Scientific Q Exactive mass
570 spectrometer run with polarity switching (+3.5 kV / -3.5 kV) in full scan mode with an m/z range of 65-
571 975. TraceFinder 4.1 (Thermo Scientific) was used to quantify the targeted metabolites by area under
572 the curve using expected retention time and accurate mass measurements (< 5 ppm). Values were
573 normalized to cell number and sample protein concentration. Relative amounts of metabolites were
574 calculated by summing up the values for all isotopologues of a given metabolite. Fractional contribution
575 (FC) of $^{13}C$ carbons to total carbon for each metabolite was calculated as previously described [57].

576 ***Data availability***

577 Newly generated single-cell sequencing data will be made public on acceptance for publication.

578

579 **References**


580 1. Buechler MB*, et al.* Cross-tissue organization of the fibroblast lineage. *Nature* **593**, 575-579
581 (2021).
582
583 2. Tsukui T*, et al.* Collagen-producing lung cell atlas identifies multiple subsets with distinct
584 localization and relevance to fibrosis. *Nat Commun* **11**, 1920 (2020).
585
586 3. Tsukui T, Wolters PJ, Sheppard D. Alveolar fibroblast lineage orchestrates lung inflammation
587 and fibrosis. *Nature* **631**, 627-634 (2024).
588
589 4. Aran D*, et al.* Reference-based analysis of lung single-cell sequencing reveals a transitional
590 profibrotic macrophage. *Nat Immunol* **20**, 163-172 (2019).
591

592 5. Larson-Casey JL, Deshane JS, Ryan AJ, Thannickal VJ, Carter AB. Macrophage Akt1 Kinase-
593 Mediated Mitophagy Modulates Apoptosis Resistance and Pulmonary Fibrosis. *Immunity* **44**,
594 582-596 (2016).
595
596 6. Satoh T*, et al.* Identification of an atypical monocyte and committed progenitor involved in
597 fibrosis. *Nature* **541**, 96-101 (2017).
598
599 7. Meinken J, Walker G, Cooper CR, Min XJ. MetazSecKB: the human and animal secretome and
600 subcellular proteome knowledgebase. *Database (Oxford)* **2015**, (2015).
601
602 8. Roofeh D*, et al.* Tocilizumab Prevents Progression of Early Systemic Sclerosis-Associated
603 Interstitial Lung Disease. *Arthritis Rheumatol* **73**, 1301-1310 (2021).
604
605 9. Group RC. Tocilizumab in patients admitted to hospital with COVID-19 (RECOVERY): a
606 randomised, controlled, open-label, platform trial. *Lancet* **397**, 1637-1645 (2021).
607
608 10. Khanna D*, et al.* Tocilizumab in systemic sclerosis: a randomised, double-blind, placebo-
609 controlled, phase 3 trial. *Lancet Respir Med* **8**, 963-974 (2020).
610
611 11. Narvaez J, J LL, Alegre Sancho JJ, Molina-Molina M, Nolla JM, Castellvi I. Effectiveness and
612 safety of tocilizumab for the treatment of refractory systemic sclerosis associated interstitial lung
613 disease: a case series. *Ann Rheum Dis* **78**, e123 (2019).
614
615 12. Riteau N*, et al.* Extracellular ATP is a danger signal activating P2X7 receptor in lung
616 inflammation and fibrosis. *Am J Respir Crit Care Med* **182**, 774-783 (2010).
617
618 13. Bhattacharyya A*, et al.* Macrophage Cx43 Is Necessary for Fibroblast Cytosolic Calcium and
619 Lung Fibrosis After Injury. *Front Immunol* **13**, 880887 (2022).
620
621 14. Trang T, Beggs S, Wan X, Salter MW. P2X4-receptor-mediated synthesis and release of brain-
622 derived neurotrophic factor in microglia is dependent on calcium and p38-mitogen-activated
623 protein kinase activation. *J Neurosci* **29**, 3518-3528 (2009).
624
625 15. Le Guilcher C*, et al.* The P2X4 purinergic receptor regulates hepatic myofibroblast activation
626 during liver fibrogenesis. *J Hepatol* **69**, 644-653 (2018).
627
628 16. Dichtl S*, et al.* Lactate and IL6 define separable paths of inflammatory metabolic adaptation. *Sci*
629 *Adv* **7**, (2021).
630
631 17. Jin S*, et al.* Inference and analysis of cell-cell communication using CellChat. *Nat Commun* **12**,
632 1088 (2021).
633
634 18. Strunz M*, et al.* Alveolar regeneration through a Krt8+ transitional stem cell state that persists in
635 human lung fibrosis. *Nat Commun* **11**, 3559 (2020).
636
637 19. Fabre T*, et al.* Identification of a broadly fibrogenic macrophage subset induced by type 3
638 inflammation. *Sci Immunol* **8**, eadd8945 (2023).
639
640 20. Steggerda SM*, et al.* Inhibition of arginase by CB-1158 blocks myeloid cell-mediated immune
641 suppression in the tumor microenvironment. *J Immunother Cancer* **5**, 101 (2017).
642

21. Tharp KM, *et al.* Myeloid mechano-metabolic programming restricts anti-tumor immunity. *bioRxiv*, 2022.2007.2014.499764 (2022).

22. Tran DH, *et al.* Mitochondrial NADP(+) is essential for proline biosynthesis during cell growth. *Nat Metab* **3**, 571-585 (2021).

23. Prasse A, *et al.* BAL Cell Gene Expression Is Indicative of Outcome and Airway Basal Cell Involvement in Idiopathic Pulmonary Fibrosis. *Am J Respir Crit Care Med* **199**, 622-630 (2019).

24. Perera LMB, *et al.* The Regulation of Skin Fibrosis in Systemic Sclerosis by Extracellular ATP via P2Y(2) Purinergic Receptor. *J Invest Dermatol* **139**, 890-899 (2019).

25. Solini A, Chiozzi P, Morelli A, Fellin R, Di Virgilio F. Human primary fibroblasts in vitro express a purinergic P2X7 receptor coupled to ion fluxes, microvesicle formation and IL-6 release. *J Cell Sci* **112 ( Pt 3)**, 297-305 (1999).

26. Mauer J, *et al.* Signaling by IL-6 promotes alternative activation of macrophages to limit endotoxemia and obesity-associated resistance to insulin. *Nat Immunol* **15**, 423-430 (2014).

27. Wang Q, *et al.* Vascular niche IL-6 induces alternative macrophage activation in glioblastoma through HIF-2alpha. *Nat Commun* **9**, 559 (2018).

28. Fernando MR, Reyes JL, Iannuzzi J, Leung G, McKay DM. The pro-inflammatory cytokine, interleukin-6, enhances the polarization of alternatively activated macrophages. *PLoS One* **9**, e94188 (2014).

29. Bhattacharya M, Ramachandran P. Immunology of human fibrosis. *Nat Immunol*, (2023).

30. Zhou X, *et al.* Circuit Design Features of a Stable Two-Cell System. *Cell* **172**, 744-757 e717 (2018).

31. Boyd DF, *et al.* Exuberant fibroblast activity compromises lung function via ADAMTS4. *Nature* **587**, 466-471 (2020).

32. Pesce JT, *et al.* Arginase-1-expressing macrophages suppress Th2 cytokine-driven inflammation and fibrosis. *PLoS Pathog* **5**, e1000371 (2009).

33. Raghu G, *et al.* SAR156597 in idiopathic pulmonary fibrosis: a phase 2 placebo-controlled study (DRI11772). *Eur Respir J* **52**, (2018).

34. Wilson MS, *et al.* Bleomycin and IL-1beta-mediated pulmonary fibrosis is IL-17A dependent. *J Exp Med* **207**, 535-552 (2010).

35. Monticelli LA, *et al.* Arginase 1 is an innate lymphoid-cell-intrinsic metabolic checkpoint controlling type 2 inflammation. *Nat Immunol* **17**, 656-665 (2016).

36. Murthy S, Larson-Casey JL, Ryan AJ, He C, Kobzik L, Carter AB. Alternative activation of macrophages and pulmonary fibrosis are modulated by scavenger receptor, macrophage receptor with collagenous structure. *FASEB J* **29**, 3527-3536 (2015).

37. Zhang H, *et al.* Annexin A2/TLR2/MYD88 pathway induces arginase 1 expression in tumor-associated neutrophils. *J Clin Invest* **132**, (2022).

38. Rotondo R, *et al.* IL-8 induces exocytosis of arginase 1 by neutrophil polymorphonuclears in nonsmall cell lung cancer. *Int J Cancer* **125**, 887-893 (2009).

39. Cane S, *et al.* Neutralization of NET-associated human ARG1 enhances cancer immunotherapy. *Sci Transl Med* **15**, eabq6221 (2023).

40. Mestas J, Hughes CC. Of mice and not men: differences between mouse and human immunology. *J Immunol* **172**, 2731-2738 (2004).

41. Foo SS, *et al.* Ephrin-B2 controls cell motility and adhesion during blood-vessel-wall assembly. *Cell* **124**, 161-173 (2006).

42. Clausen BE, Burkhardt C, Reith W, Renkawitz R, Forster I. Conditional gene targeting in macrophages and granulocytes using LysMcre mice. *Transgenic Res* **8**, 265-277 (1999).

43. Ozaki T, *et al.* The P2X4 receptor is required for neuroprotection via ischemic preconditioning. *Sci Rep* **6**, 25893 (2016).

44. El Kasmi KC, *et al.* Toll-like receptor-induced arginase 1 in macrophages thwarts effective immunity against intracellular pathogens. *Nat Immunol* **9**, 1399-1406 (2008).

45. Yata Y, *et al.* DNase I-hypersensitive sites enhance alpha1(I) collagen gene expression in hepatic stellate cells. *Hepatology* **37**, 267-276 (2003).

46. Schneider C, *et al.* Tissue-Resident Group 2 Innate Lymphoid Cells Differentiate by Layered Ontogeny and In Situ Perinatal Priming. *Immunity* **50**, 1425-1438 e1425 (2019).

47. Reese TA, *et al.* Chitin induces accumulation in tissue of innate immune cells associated with allergy. *Nature* **447**, 92-96 (2007).

48. Kopf M, *et al.* Impaired immune and acute-phase responses in interleukin-6-deficient mice. *Nature* **368**, 339-342 (1994).

49. Bankhead P, *et al.* QuPath: Open source software for digital pathology image analysis. *Sci Rep* **7**, 16878 (2017).

50. Hao Y, *et al.* Integrated analysis of multimodal single-cell data. *Cell* **184**, 3573-3587 e3529 (2021).

51. McGinnis CS, Murrow LM, Gartner ZJ. DoubletFinder: Doublet Detection in Single-Cell RNA Sequencing Data Using Artificial Nearest Neighbors. *Cell Syst* **8**, 329-337 e324 (2019).

52. Heng TS, Painter MW, Immunological Genome Project C. The Immunological Genome Project: networks of gene expression in immune cells. *Nat Immunol* **9**, 1091-1094 (2008).

53. Chen EY, *et al.* Enrichr: interactive and collaborative HTML5 gene list enrichment analysis tool. *BMC Bioinformatics* **14**, 128 (2013).

54. Gene Ontology C*, et al.* The Gene Ontology knowledgebase in 2023. *Genetics* **224**, (2023).

55. Kramer A, Green J, Pollard J, Jr., Tugendreich S. Causal analysis approaches in Ingenuity Pathway Analysis. *Bioinformatics* **30**, 523-530 (2014).

56. Palla G*, et al.* Squidpy: a scalable framework for spatial omics analysis. *Nat Methods* **19**, 171-178 (2022).

57. Robinson MD, Oshlack A. A scaling normalization method for differential expression analysis of RNA-seq data. *Genome Biol* **11**, R25 (2010).

58. Satija R, Farrell JA, Gennert D, Schier AF, Regev A. Spatial reconstruction of single-cell gene expression data. *Nat Biotechnol* **33**, 495-502 (2015).

## Acknowledgements

This work was supported by funding from the US Department of Defense (Grant W81XWH2110417 to MB), the UCSF Bakar Aging Research Institute (Investigator Grant to MB), Longevity Impetus Grants from Norn Group (MB and JGO), the Nina Ireland Program for Lung Health Innovative Grant Program (PY), and NIH (1R01HL142701-01 to ABM). The authors would like to acknowledge the staff within the Biological Imaging Development CoLab (BIDC) at UCSF Parnassus Heights, particularly Kyle Marchuk and Austin Edwards, for their support in microscopy experiments. Sequencing performed at the UCSF CAT was supported by UCSF PBBR, RRP IMIA, and NIH 1S10OD028511-01. We are grateful to Dr. Clifford Lowell for his valuable comments and suggestions on the manuscript. We thank Giovanni Palla and Nathan Levy for help in extending the Squidpy package.

## Author contributions

PY performed or assisted in the analysis of all the experiments and in figure preparation. JGO performed single cell sequencing experiments and analysis and figure preparation. KC and SP performed single cell library preparation and sequencing, supervised by ARA. NB and AB assisted in functional experiments with lung tissues and cells. XY performed human cell coculture experiments under the supervision of BL. JN performed flow cytometry of mouse lung cells supervised by ABM. KB, TJ, and JW performed mouse breeding and development of crosses for experiments. TT and DS

assisted in analysis of single cell sequencing data from mouse lung fibroblasts. MM and HT provided deceased donor control lung tissues supervised by MAM. LP and AG performed Xenium spatial transcriptomic analysis supervised by WE. CC and AW designed and implemented spatial proximity analysis of Xenium data. RM generated and provided P2x4 floxed mice. WT and ST performed MIBI analysis under the guidance of TB. PJW provided lung explants from IPF patients and helped to interpret associated imaging data. KMT designed and performed metabolomic assays, assisted by PY. MB conceived of the work, supervised experimental planning and execution, and wrote the manuscript with input from PJW, DS, and KMT.

**Materials and Correspondence**

Correspondence to mallar.bhattacharya@ucsf.edu.

Figure 1: P2rx4 regulates fibroblast IL-6 expression.

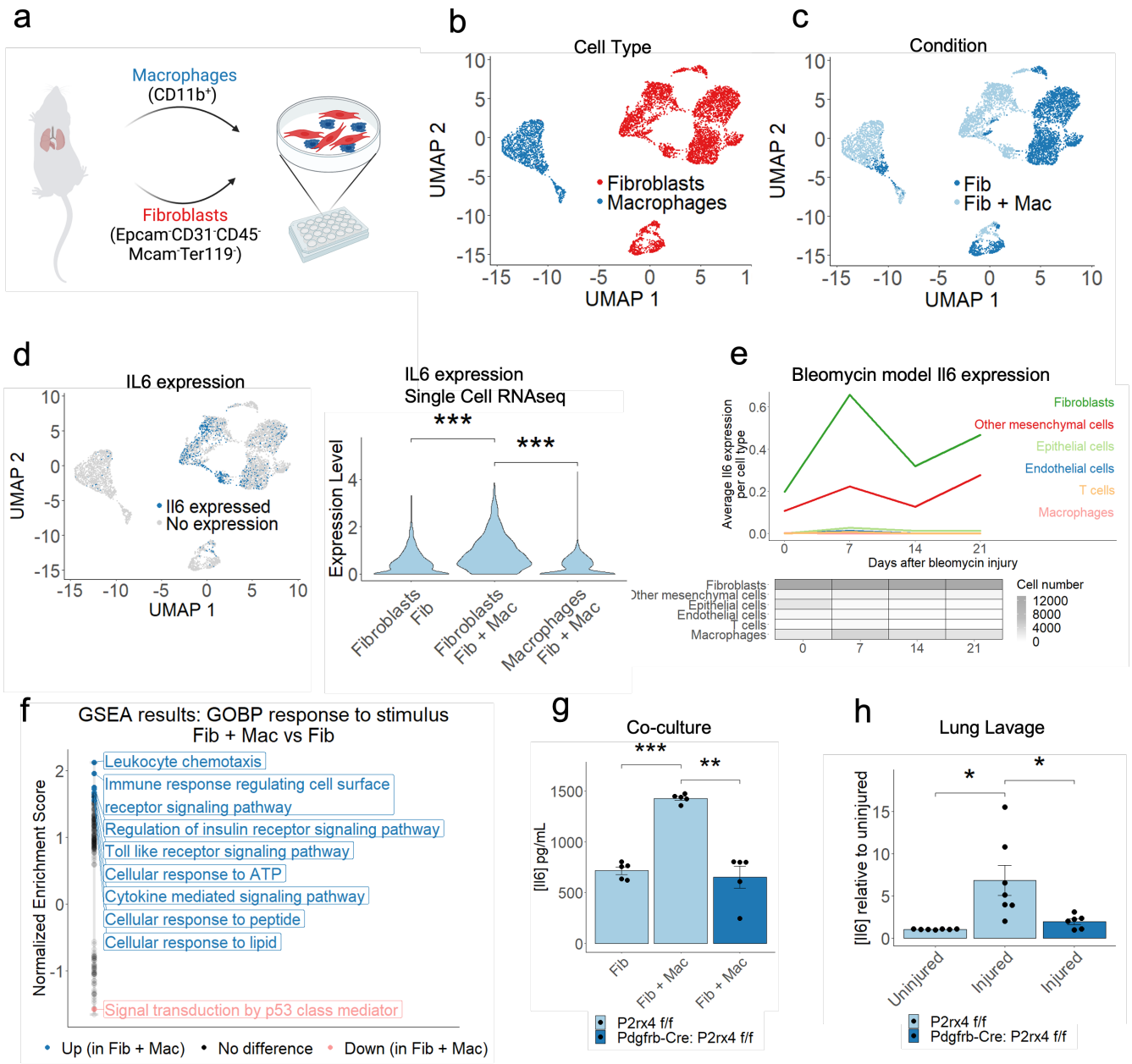


**Figure 1: P2rx4 regulates fibroblast IL-6 expression.**

(a) Schematic of scRNAseq of primary lung macrophage and fibroblast coculture.
(b) UMAP plot of scRNAseq for macrophage-fibroblast cocultures with SingleR-based cell type annotation [4] shown. Data represent n=2 separate cultures for each condition.
(c) UMAP plot for data from (b) showing sample of origin ("Fib"=fibroblast monoculture, "Fib + Mac"= fibroblast coculture with macrophages).
(d) Left: UMAP plot showing *Il6* expression. Right: Violin plot of *Il6 expression*. ***p<0.001 by Wilcoxon Rank Sum test corrected for multiple comparisons by Bonferroni method.

(e) Quantification of *Il6* expression by cell type in cells sequenced by scRNAseq directly after isolation from the lung at steady state and multiple time points after injury (reanalysis of merged data[3, 18] normalized by Sctransform[58]).

(f) Gene set enrichment analysis (GSEA) of fibroblast single cell transcriptomes in coculture with macrophages compared to fibroblast monoculture using GO “Response to stimulus” pathways.

(g) IL-6 ELISA of conditioned media from macrophage-fibroblast cocultures with or without fibroblast-specific P2rx4 deletion. N=5 five biological replicates per condition. **$p<0.01$, ***$p<0.001$ by Student’s t-test. Bars shows +/- SEM.

(h) IL-6 ELISA from bronchoalveolar lavage from mice with or without fibroblast-specific P2rx4 deletion. N=7, 7, 6 biological replicates, left to right. *$p<0.05$ by Student’s t-test. Bars shows +/- SEM.

Figure 2: IL-6 is required for Arg1 expression in profibrotic macrophages.

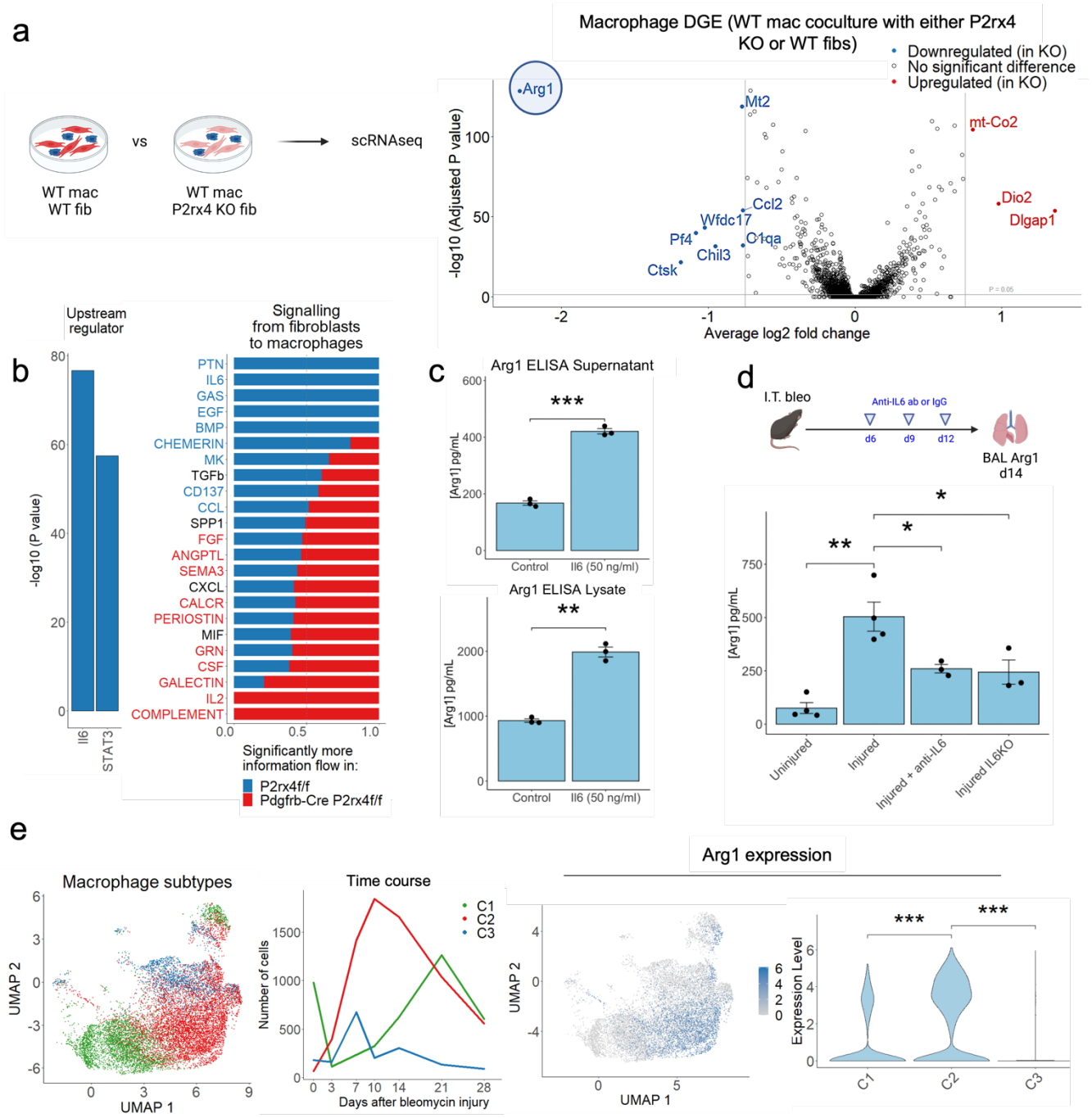


**Figure 2: IL-6 signaling regulates Arg1 expression in profibrotic macrophages.**

(a) Schematic of design of co-culture scRNAseq and volcano plot for macrophages from scRNAseq of macrophage-fibroblast cocultures for WT macrophages and fibroblasts, or WT macrophages cocultured with P2rx4 KO (*Pdgfrb-Cre: P2rx4 f/f*) fibroblasts. Significance was determined by Wilcoxon Rank Sum test corrected for multiple comparisons by Bonferroni method. Color-

821 labeled genes had $p<0.05$ and absolute value of log2 fold change >0.75. Data represent n=2
822 separate cocultures.
823 (b) Left: Ingenuity Pathways Analysis of predicted upstream regulators for macrophages cultured
824 with WT relative to P2rx4 fibroblasts. Right: CellChat plot comparing WT and P2rx4 conditions
825 for data from Figure 2a. Significance was determined by Wilcoxon test with $p<0.05$.
826 (c) Arg1 ELISA of cell lysates and conditioned media collected from mouse lung macrophage
827 monoculture 72 hours after IL-6 treatment. N=3 biological replicates per condition.**$p<0.01$,
828 ***$p<0.001$ by Student's t-test. Bars shows +/- SEM.
829 (d) Arg1 ELISA of bronchoalveolar lavage fluid taken at day 14 from bleomycin-injured mice treated
830 with anti-IL-6 antibody or IgG control, or from IL-6 KO injured mice. N=4, 4, 3, and 3 biological
831 replicates per condition. *$p<0.05$ by Student's t-test, **$p<0.01$. Bars shows +/- SEM.
832 (e) Analysis of macrophages from bleomycin lung injury (data reanalyzed from[18]). Left: Annotation
833 of macrophages from multiple time points, according to C1, C2, or C3 macrophage annotation
834 (as described in [4]; C1=alveolar macrophages; C2=transitional monocyte-derived macrophages;
835 C3=monocyte derived macrophages). Center: Proportions of C1, C2, and C3 across time. Right
836 Feature plot of Arg1 expression and violin plot of Arg1 expression according to cluster (C1, C2,
837 and C3). ***$p<0.001$ by Student's t-test.
838
839
840

Figure 3: Arg1 is necessary for lung fibrosis.

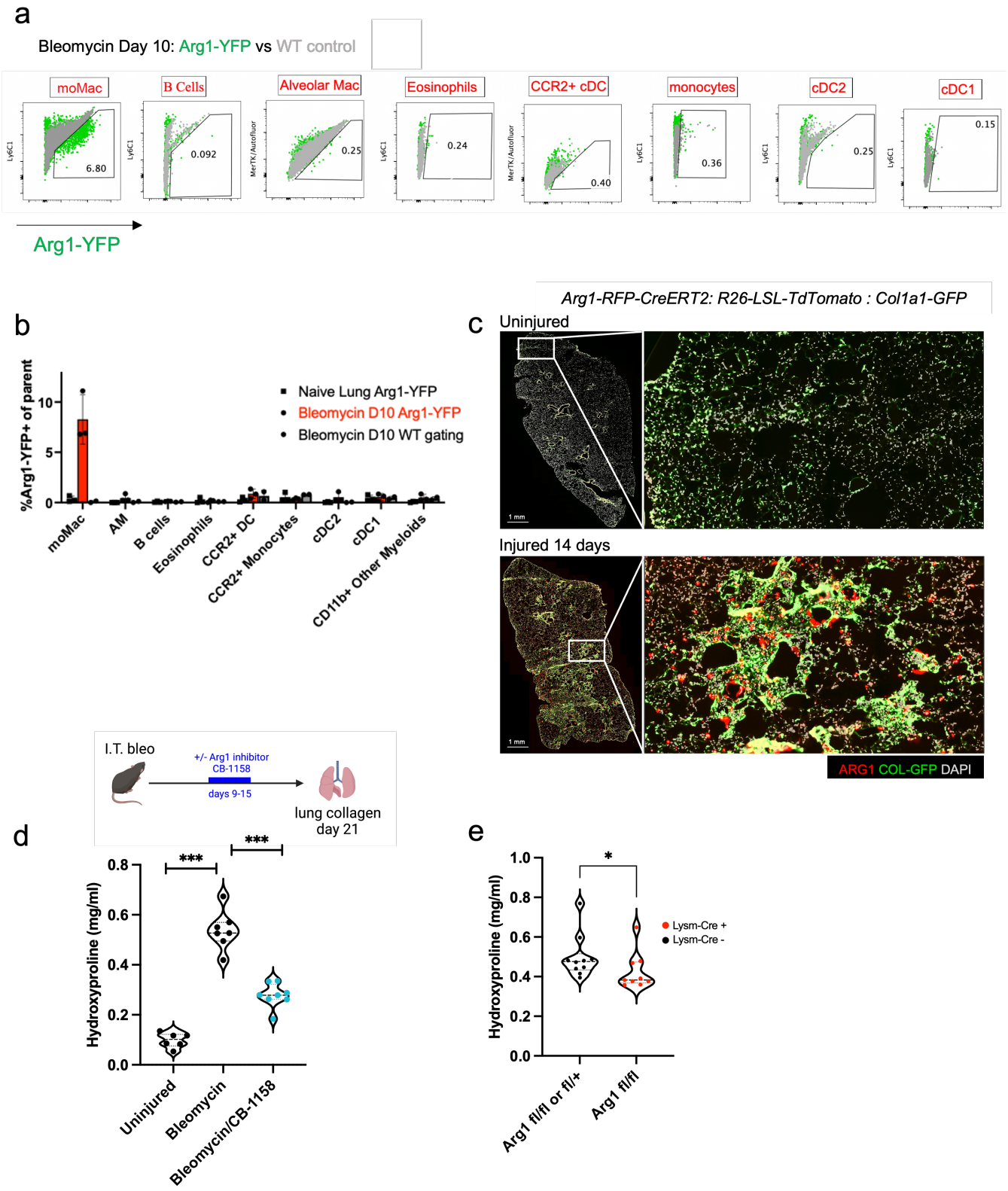

843 **Figure 3: Arg1 is necessary for lung fibrosis.**

844 (a) Representative flow cytometry of mouse lungs from Arg1-YFP reporter and WT mice at steady
845 state and 10 days post-bleomycin. MoMac=monocyte-derived macrophage (CD64+CD11b+
846 SiglecF-). AM=alveolar macrophage (CD64+SiglecF+).

847 (b) Plot of percentage of cells expressing YFP in each lineage. N=3 mice per condition.

848 (c) Immunofluorescence of *Col1a1-GFP* mice labeled with Arg1 antibody at 14 days after
849 bleomycin injury.

850 (d) Hydroxyproline assay for collagen content of lungs from injured and uninjured WT mice treated
851 with or without Arg1 inhibitor CB-1158 during days 9-15 post bleomycin. N=6, 7, 8 mice, left to
852 right. ***$p<0.001$ by Student's t-test. Bars shows +/- SEM.

853 (e) Hydroxyproline assay for collagen content of lungs from mice 21 days after bleomycin injury.
854 N=10 and 9 mice, left to right. *$p<0.05$ by Mann-Whitney test.

855
856
857

Figure 4: Arg1-dependent ornithine induces fibroblast collagen expression.

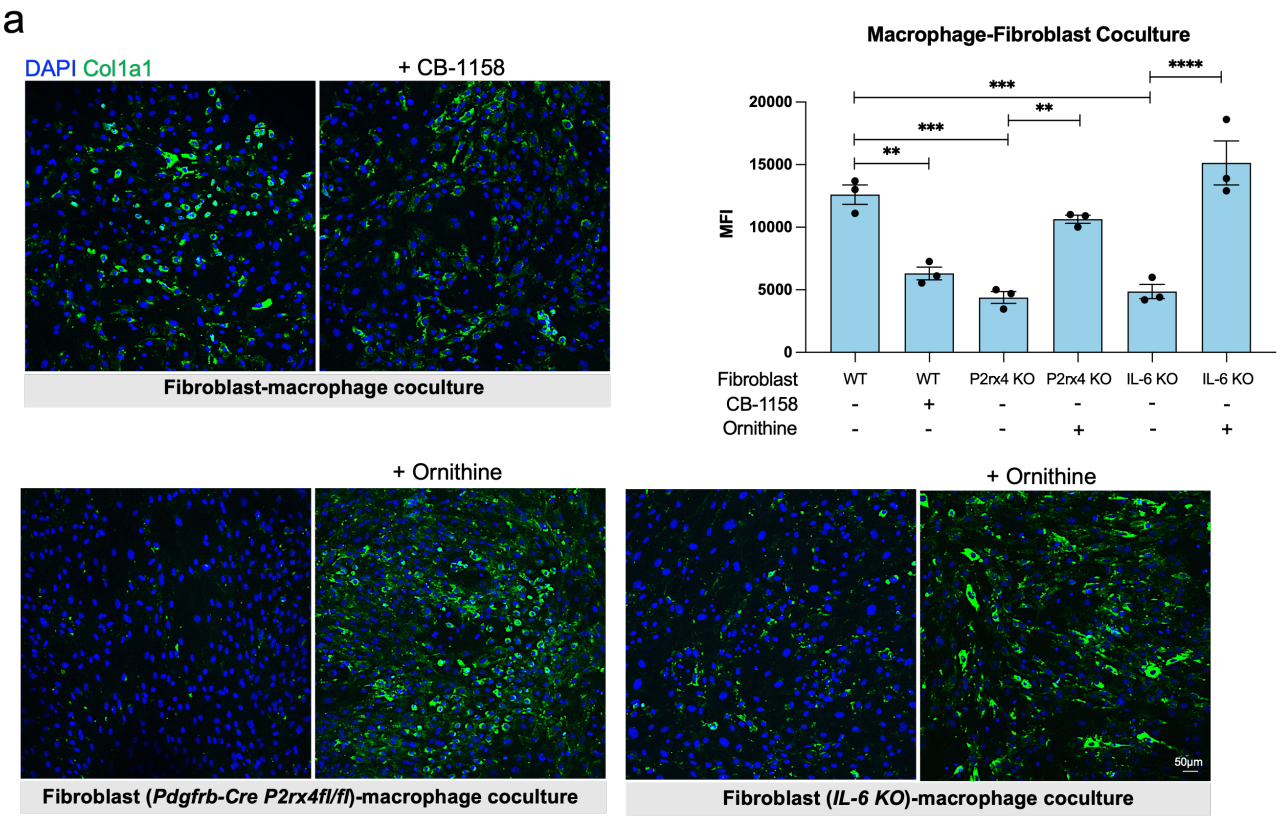


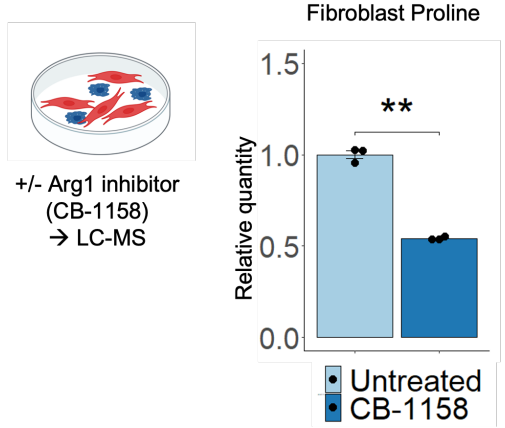


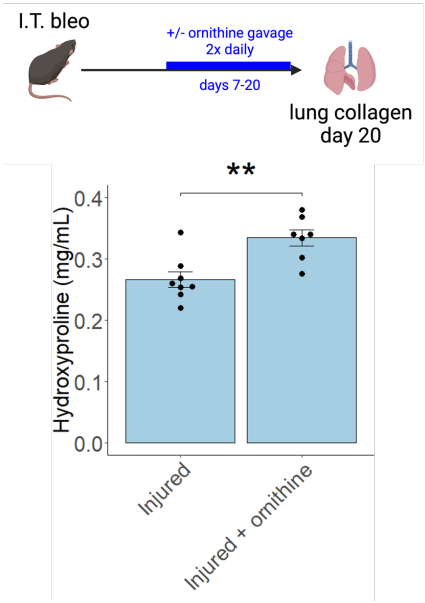

862 **Figure 4: Arg1-dependent ornithine induces fibroblast collagen expression.**

863 (a) Representative samples of Col1a1 immunofluorescence of mouse fibroblast cocultures or
864 macrophage-fibroblast cocultures with or without CB-1158 or ornithine treatment. Quantitation is
865 for N=3 biological replicates per condition. *p<0.05 by 1-way ANOVA with post hoc Sidak's
866 multiple comparisons tests. **p<0.01, ***p<0.001, ****p<0.0001. Bars shows +/- SEM.

867 (b) Relative quantities of proline in lysates of murine primary lung fibroblasts isolated after coculture
868 with macrophages, with or without CB-1158 inhibitor treatment, quantified by liquid
869 chromatography-mass spectrometry. N=3 biological replicates for macrophages and fibroblasts,
870 respectively. **p<0.01 by Student's t-test.

871 (c) Hydroxyproline assay for collagen content of lungs from injured WT mice treated with or without
872 ornithine (2 mg/kg) twice daily by ornithine gavage during days 7 through 20 . N=8, 7 mice, left
873 to right. **p<0.01 by Student's t-test. Bars shows +/- SEM.

874
875
876

Figure 5: ARG1 is expressed in IPF myeloid cells and regulates collagen expression.

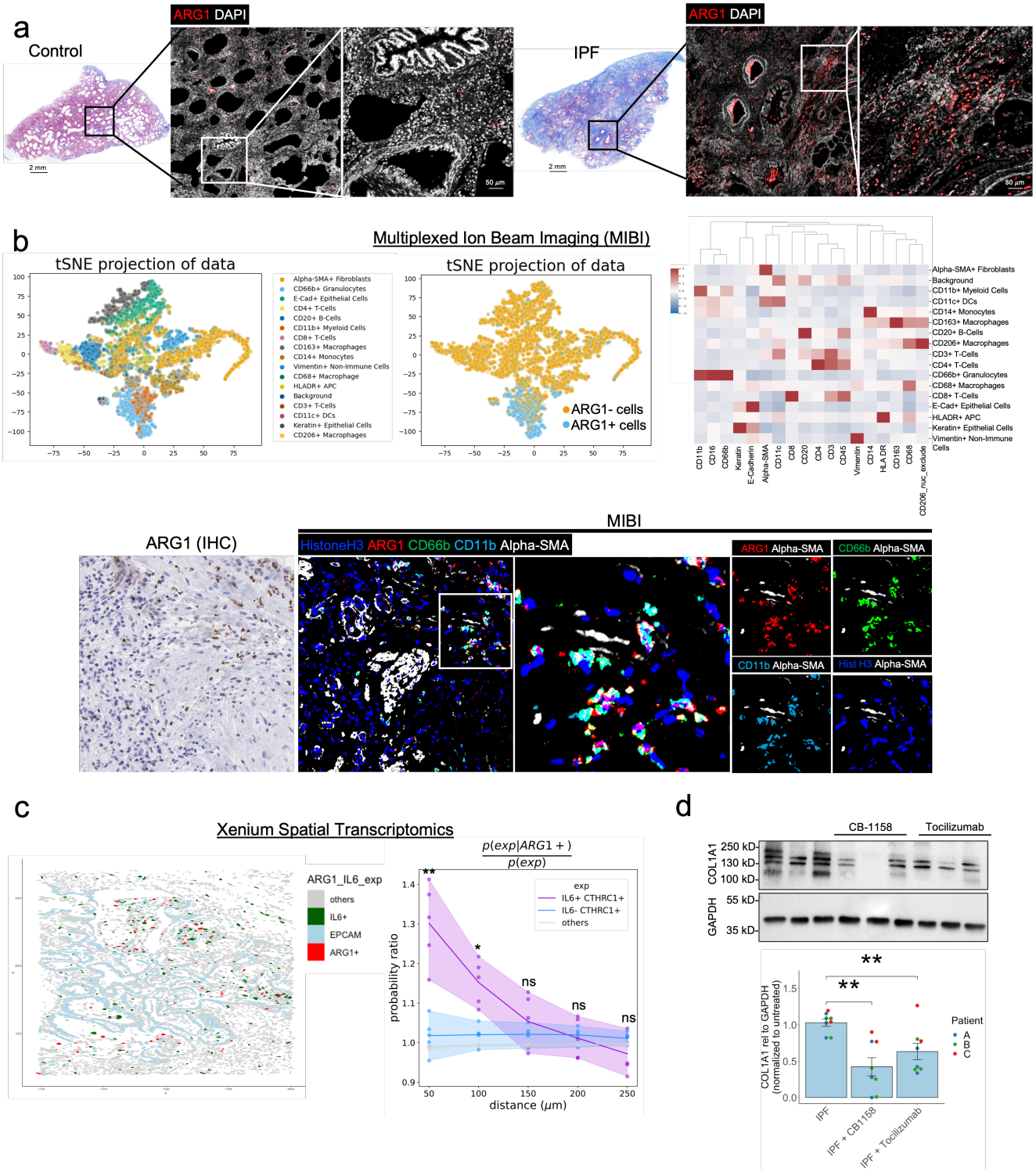


**Figure 5: ARG1 is expressed in IPF myeloid cells and regulates collagen expression.**

(a) Representative immunofluorescence of human lung IPF and healthy control sections (n=4 and n=2, respectively) for ARG1, with Masson's fibrosis stain of an adjacent section. The region of

882 magnification is from the approximate area of a separate section that was imaged with
883 Masson's trichrome histologic stain for fibrosis.
884 (b) Multiplexed ion beam imaging (MIBI) analysis: Top, left and middle: tSNE projections
885 corresponding to 2 IPF samples. Top, right: Heat map of marker expression for each
886 phenotype cluster with indicated Z-score. Bottom, left: ARG1 immunostaining of representative
887 IPF sample. Bottom, right: Multichannel MIBI image of a representative field of view with
888 ARG1, CD66B, CD11B, alpha-SMA, and Histone H3 expression.
889 (c) 10x Xenium spatial analysis: Left: Representative field of view showing cells expressing ARG1,
890 IL6, and EPCAM. Right: Proximity analysis of Xenium data plotting the probability ratio, P(exp |
891 Arg1+)/P(exp), defined as the average probability of encountering an IL6+CTHRC1+ fibroblast,
892 an IL6-CTHRC1+ fibroblast, or other cells computed at multiple radial distances from ARG1+
893 cells, normalized by the probability of a cell being positive for the markers in question (see
894 Methods). 50% random subsampling of the entire tissue sample was performed 5 times, and
895 for each subsample, a probability ratio for each marker was computed for each distance. The
896 solid lines are averages, and the shaded regions are bounded by the minimum and maximum
897 probability ratio generated by the subsamples. **$p<0.01$ and *$p<0.05$ by paired one-way
898 ANOVA with post hoc Sidak's multiple comparisons tests. The plot presents data from a patient
899 that is representative of findings from n=2 separate patients.
900 (d) Immunoblot for COL1A1 from lung slice lysates prepared 24 hours after treatment in culture
901 with the indicated inhibitors. Quantitation is for n=3 patients. **$p<0.01$ by Student's t-test. Bars
902 shows +/- SEM.
903
904